Journal of Alloys and Compounds 521 (2012) 30–34

Contents lists available at SciVerse ScienceDirect

Journal of Alloys and Compounds

journal homepage: www.elsevier.com/locate/jallcom

Enhanced low field magnetoresistance in $La_{0.7}Sr_{0.3}MnO_3$–La_2O_3 composites

Hyo-Jin Kim, Sang-Im Yoo*

Department of Materials Science and Engineering, Seoul National University, Research Institute of Advanced Materials (RIAM), Seoul 151-744, Republic of Korea

ARTICLE INFO

Article history:
Received 2 September 2011
Received in revised form
21 December 2011
Accepted 23 December 2011
Available online 13 January 2012

Keywords:
Low-field magnetoresistance (LFMR)
$La_{0.7}Sr_{0.3}MnO_3$ (LSMO)–La_2O_3 composite
Spin-dependent scattering

ABSTRACT

A significant enhancement of low-field magnetoresistance (LFMR) was obtainable from the polycrystalline composites between $La_{0.7}Sr_{0.3}MnO_3$ (LSMO) and La_2O_3 phases. For this study, the magnetic and magnetotransport properties of samples with various compositions of $(1-x)$LSMO–xLa_2O_3 (x = 0, 0.025, 0.05, 0.075, 0.1, 0.2, 0.3) were systematically investigated. Compared with pure LSMO (T_C = 362 K), all composites exhibited a slightly depressed T_C values of 355–358 K, implying that the magnetic ordering of LSMO is insignificantly affected by chemically compatible La_2O_3. While the LFMR value at 300 K in 500 Oe was monotonously increased from 1.36 to 1.67% with increasing x from 0 to 0.075, it was abruptly increased to the maximum value of 2.22% for x = 0.1 with only one order increase in its resistivity relative to x = 0.075, and further increasing x from 0.1 to 0.3 resulted in a linear decrease to 1.8% with almost no variation in resistivity. This peculiar behavior, different from normal metallic percolation threshold effect, is closely related to the microstructure variation. Remarkably improved LFMR properties of the LSMO–La_2O_3 composite samples are attributed to high grain boundary areal density and sharpening of a disordered LSMO grain boundary region acting as more effective spin-dependent scattering centers.

1. Introduction

$RE_{1-x}A_xMnO_3$ perovskite manganites (where RE is a rare earth element and A is a divalent cation), exhibiting the colossal magnetoresistance (CMR) effect, have drawn a considerable attention in recent years because of their abundant physical properties and potential applications such as magnetoresistive transducers and sensors [1,2]. LSMO is one of the most attractive CMR materials since it has high Curie temperature ($T_C \approx 360$ K) which makes it possible to fabricate devices operating at room temperature [3,4]. The MR effects of LSMO polycrystalline materials have two types of high-field and low-field MR, depending on their origin [5–8]. The high field MR (HFMR) effect is observable at the temperatures below T_C only in high fields (>1 T). The HFMR effect originates from the existence of a noncollinear spin structure in the surface layer. On the other hand, a low field MR (LFMR) effect can be observed at the temperatures below T_C in low fields (<0.2 T). The LFMR effect is attributed to a spin-polarized tunneling at the grain boundaries. Thus, it is very important to control the grain boundary properties of LSMO polycrystalline samples for the enhancement of LFMR.

Since LFMR is applicable to magnetic devices, many groups have attempted to improve the LFMR effect by making a composite of manganites with second phases such as insulators [9–17], metals [18,19], polymers [20,21], and other manganites [22–24]. The second phases usually obstruct the magnetic spin alignment near the grain boundary of the manganite. The improvement of LFMR in the perovskite manganite-oxide composites is normally accompanied by a significant increase in their electrical resistivities by several orders of magnitude higher than that of pure polycrystalline manganite and an abrupt decrease in T_C. To avoid such a serious degradation both in T_C and electrical conductivity, we have tried to select the second phases chemically compatible with LSMO. Referring to the La_2O_3–Mn_2O_3 phase diagram reported by van Roosmalen et al. [25], one can see that both Mn_2O_3 (or Mn_3O_4) and La_2O_3 are chemically compatible with $LaMnO_{3+d}$ solid solution phases. For the LSMO–manganese oxide composites, we reported a successful achievement of the highest LFMR value of 1.7% at 500 Oe with the maximum dMR/dH value of 28.3% k Oe^{-1} at 300 K without a significant variation in T_C and resistivity [26]. In this study, La_2O_3 was selected as an alternative second phase chemically compatible with LSMO. We here report that it is possible to obtain a high LFMR effect from the LSMO–La_2O_3 composite at room temperature as well.

2. Experimental

Samples were prepared by using the conventional solid-state reaction. The nominal composition of samples was $(1-x)$LSMO–xLa_2O_3 (x = 0, 0.025, 0.05, 0.075, 0.1, 0.2, 0.3). The precursor materials were Mn_2O_3, La_2O_3, and $SrCO_3$ powders with all 99.9% purity. The precursors were weighed and ball-milled in ethyl alcohol using ZrO_2 balls for 24 h. The ball-milled slurry was dried and calcined twice at 1100 °C for 8 h in air. As-calcined powder were uniaxially pressed into pellets with diameter of 10 mm, and then followed by cold isostatic pressing (~2 ton cm^{-2}). The pellets were sintered at 1400 °C for 8 h in air with a heating rate of 5 °C min^{-1}. High

* Corresponding author. Tel.: +82 2 880 5720; fax: +82 2 885 9671.
E-mail addresses: fyolove@snu.ac.kr (H.-J. Kim), siyoo@snu.ac.kr (S.-I. Yoo).

0925-8388/$ – see front matter © 2011 Elsevier B.V. All rights reserved.
doi:10.1016/j.jallcom.2011.12.121

resolution X-ray diffraction (XRD, BRUKER D8 ADVANCE) with θ–2θ scan using Cu-K_α radiation ($\lambda = 1.54$ Å) and scanning electron microscopy (SEM, JEOL JSM-6360) were performed for phase and microstructure analysis, respectively. Temperature and field dependencies of magnetism were measurement with a superconducting quantum interference device (SQUID) magnetometer (MPMS XL5, Quantum Design). The M–T curves were measured with a field-cooled warming procedure under the applied field of 100 Oe. Measurements of LFMR properties were performed using the standard four probe method within the SQUID magnetometer. Both the electrical current and magnetic field were applied along the long dimension of samples. The Curie temperatures of samples were determined by the maximum point of $|dM/dT|$ in the M versus T curves.

3. Results and discussion

Fig. 1 shows the powder XRD patterns of pure LSMO and $(1-x)$LSMO–xLa$_2$O$_3$ ($x = 0.025$, 0.05, 0.075, 0.1, 0.2, and 0.3) composite samples. As can be seen in Fig. 1, the relative peak intensity of La_2O_3 is gradually increased with increasing La_2O_3 mole fraction and other second phases are unobservable, representing that LSMO and La_2O_3 phases are chemically compatible. Referring to the La_2O_3–Mn_2O_3 binary phase diagram [25], $LaMnO_3$ is expected

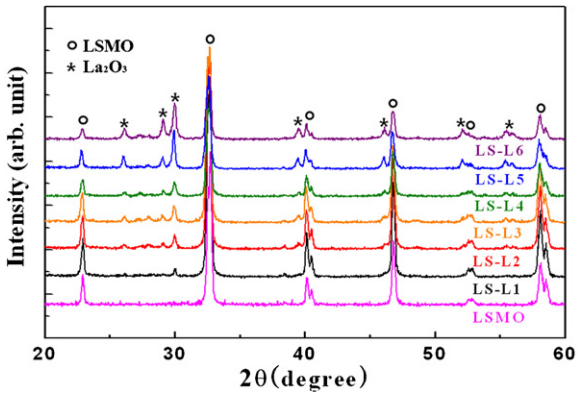

Fig. 1. XRD patterns of pure LSMO and LSMO–La_2O_3 composites.

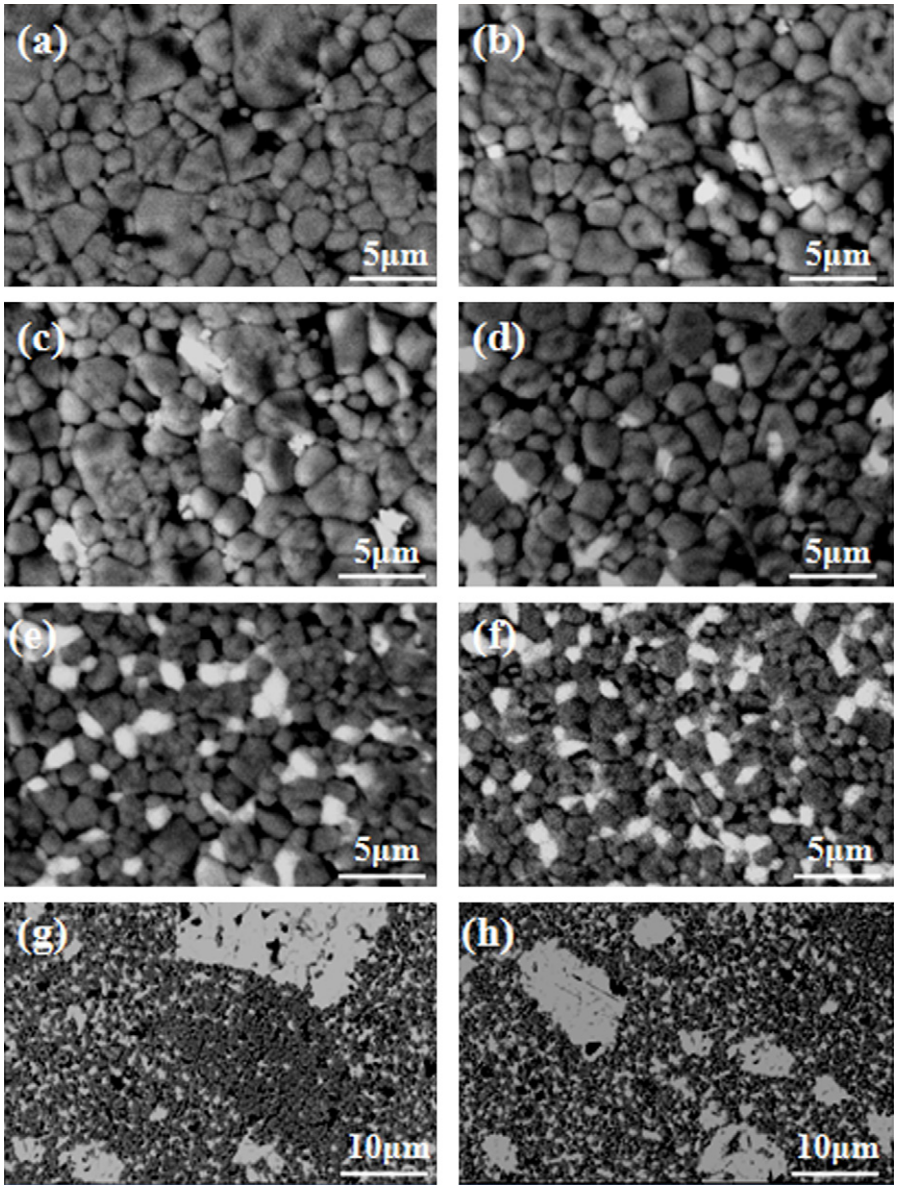

Fig. 2. SEM back-scattered electron images of samples: (a) LSMO, (b) LS–L1, (c) LS–L2, (d) LS–L3 (e) LS–L4, and (f) LS–L5. Low magnification micrographs are for the samples of (g) LS–L5 and (h) LS–L6.

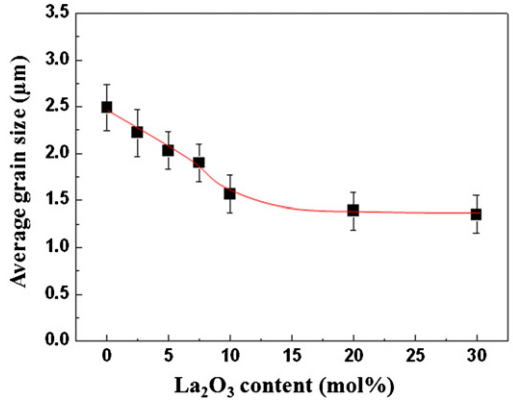

Fig. 3. The average LSMO grain size of samples as a function of the La_2O_3 content.

to react with La_2O_3 to form the $La_{1+d}MnO_3$-type solid solution at the sintering temperature of 1400 °C. However, the formation of $(La_{0.7+d},Sr_{0.3})MnO_3$-type solid solution was hardly detectable in our composite samples. In Fig. 1, it is observed that a small peak of La_2O_3 exists even in the LS–L1 sample having 2.5 mol% La_2O_3. In addition, no peak shift in the LSMO phase was detectable in the LSMO–La_2O_3 composite samples, implying that the cell parameters of the LSMO phase were unaltered after forming the composites. Therefore, it can be suggested that the solubility limit d of La^{3+} in $(La_{0.7+d},Sr_{0.3})MnO_3$ is very small.

The SEM micrographs of pure LSMO and LSMO–La_2O_3 composite samples are shown in Fig. 2. The LSMO and La_2O_3 phases in composites are clearly observed as dark and bright contrasts, respectively. From the SEM micrographs, it is obvious that the La_2O_3 particles are randomly distributed at the LSMO grain boundary up to 10 mol% La_2O_3. Interestingly, however, composites containing 20 and 30 mol% La_2O_3 resulted in a non-uniform microstructure including large agglomerated La_2O_3 grains as shown in low magnification micrographs of Fig. 2(g) and (h).

Fig. 3 shows the variation in the average grain size of LSMO grains as a function of La_2O_3 content for all samples, where the average LSMO grain size was analyzed by an image analyzer. It is shown that while the average grain size of LSMO is almost linearly decreased from 2.5 to 1.6 μm with increasing the amount of La_2O_3 up to 10 mol% La_2O_3, it is slightly decreased to 1.4 μm with further increasing the amount of La_2O_3 up to 30 mol%.

The temperature dependency of the magnetization for all samples is shown in Fig. 4. One can see that the effect of La_2O_3 addition on the paramagnetic–ferromagnetic transition temperature is insignificant. The T_C values of all samples are listed in Table 1. The T_C values of the composite samples are slightly depressed into the region of 355–358 K compared with that of pure LSMO (362 K), which might be caused by the formation of $La_{0.7+d}Sr_{0.3}MnO_3$ solid solution with a very limited d value. Although not presented, we also measured the temperature dependence of resistivity for all samples. The metal-insulator transition temperatures (T_{MI}) are listed in Table 1. Except the LSMO sample exhibiting relatively high T_{MI} value of (377 K), those of all other composite samples are in the region of 353–364 K, implying that the grain boundary disorder of LSMO grains is insignificantly affected by varying the La_2O_3 content. These results are quite different from the additive effect of perovskite manganite-oxide composites [9,10,14–17,22]. The ferromagnetic ordering of LSMO is usually weakened by the addition of a secondary phase because of its chemical reaction with LSMO resulting in the magnetic dilution [17]. Like the LSMO–manganese composites [26], however, the ferromagnetic ordering of the LSMO phase is insignificantly affected by the addition of La_2O_3 since LSMO is chemically compatible with La_2O_3.

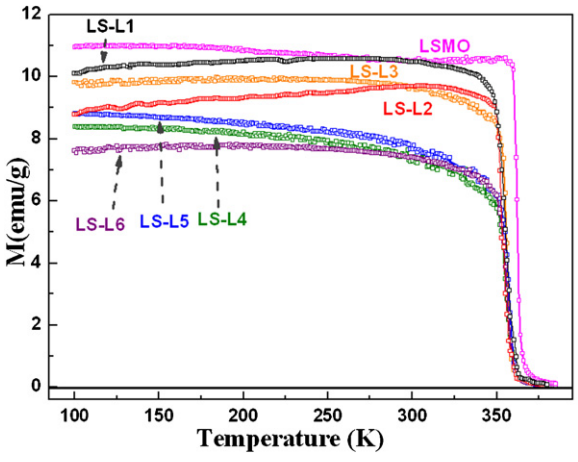

Fig. 4. Temperature dependence of magnetization for samples. The M–T curves were measured with field-cooled warming procedure under the applied field of 100 Oe.

The LFMR values of samples are represented in Fig. 5(a) and (b). For a clarity, we displayed the LFMR data of some selected samples which were not seriously overlapped each other. The LFMR values at 100 and 300 K were evaluated using the equations of $MR(\%) = (R_H - R_{H=1500\,Oe})/R_{H=1500\,Oe} \times 100\%$ and $(R_H - R_{H=500\,Oe})/R_{H=500\,Oe} \times 100\%$, respectively. The magnetotransport properties of all samples measured in this study are summarized in Table 1. The resistivity and LFMR values in Table 1 were plotted as a function of La_2O_3 content in Fig. 5(c) and (d). First of all, as shown in Fig. 5(c) and (d), while the resistivity values of the LSMO–La_2O_3 composites at the temperatures of 100 and 300 K slightly increase with increasing x from 0 to 7.5 mol%, an order of magnitude increase in resistivity occurs at x = 10 mol%, and then it slightly increases with increasing x further up to 30 mol%. This behavior can be understood as the following. The resistivity increase less than three times up to 7.5 mol% addition implies that a metallic percolation path between LSMO grains might not be seriously blocked by the insulating La_2O_3 grains. The abrupt resistivity increase from 7.5 to 10 mol% addition suggests that an effective cross-section of the metallic percolation path is reduced to one tenth, which might be due to more homogeneous distribution of La_2O_3 grains in Fig. 2(e) compared with that in Fig. 2(d). The resistivity increase from 10 to 30 mol% La_2O_3 addition is unexpectedly small, which is obviously attributed to a non-uniform distribution of La_2O_3 grains observed for 20 and 30 mol% additions as shown in Fig. 2(g) and (h), where large agglomerated La_2O_3 particles are found. One can see that the microstructures of Fig. 2(e) and (f) are almost identical except large agglomerated La_2O_3 grains shown in Fig. 2(g) (low magnification micrograph for the same 20 mol% addition with Fig. 2(f)), implying that an additional block of the metallic percolation path is simply due to large agglomerated La_2O_3 grains. If we assume that La_2O_3 particles were not agglomerated, the percolation path would be blocked much more effectively, leading to higher resistivity. Therefore, unexpectedly small increase in resistivity is attributable to the non-uniform microstructures for 20 and 30 mol% La_2O_3 additions.

On the other hand, the LFMR values at 100 K in 1500 Oe and 300 K in 500 Oe are also represented as a function of the La_2O_3 content in Fig. 5(c) and (d). While the LFMR value at 300 K in 500 Oe is monotonously increased from 1.36 to 1.67% with increasing x from 0 to 7.5 mol% La_2O_3 addition, it is abruptly increased to 2.22% for x = 10 mol%. Further increase in x from 10 to 30 mol% results in a linear decrease to 1.8%. Hence, the maximum LFMR value of 2.22% at 300 K in 500 Oe can be achieved from the LS–L4 composite of x = 0.1. Different from the behavior of the LFMR values in Fig. 5(c) and (d), the maximum dMR/dH values of samples in Table 1 are unaltered up

Table 1
Sample identification (ID) and properties of LSMO and LSMO–La_2O_3 composites: Curie temperature (T_C), metal-insulator transition temperature (T_{MI}), electrical resistivity (ρ), LFMR at 100 and 300 K in 1500 and 500 Oe, respectively, and the maximum MR change (dMR/dH) at 300 K in 500 Oe.

Sample ID	LSMO	LS–L1	LS–L2	LS–L3	LS–L4	LS–L5	LS–L6
x (mol%)	0	2.5	5	7.5	10	20	30
T_C (K)	362	356	358	356	355	358	356
T_{MI} (K)	377	363	361	364	360	354	353
LFMR (%) at 100 K	17.34	18.35	18.90	19.77	22.40	22.30	22.34
LFMR (%) at 300 K	1.36	1.37	1.63	1.67	2.22	1.99	1.80
ρ_{100K} (Ω cm)	0.0039	0.0118	0.0120	0.0122	0.130	0.180	0.181
ρ_{300K} (Ω cm)	0.0124	0.0309	0.0294	0.0320	0.328	0.342	0.348
dMR/dH (%/k Oe^{-1})	1.10	1.11	2.17	3.10	3.21	3.40	3.98

to x = 2.5 mol%, significantly increased for the composition region of x = 2.5–7.5 mol%, and then slightly increased up to x = 30 mol%. Previous literature [10,13,26,27] reported that the maximum LFMR values of the manganite composites were achievable near a metallic percolation threshold, where their resistivity values were drastically increased (normally over 10^2 Ω cm). However, the maximum LFMR values at 100 and 300 K shown in Fig. 5(c) and (d) occur at low resistivity level (<1 Ω cm) far below the metallic percolation threshold (see Table 1), implying that the maximum LFMR value of the composite with 10 mol% La_2O_3 is irrelevant to metallic percolation threshold. Instead, this peculiar behavior must be closely related to the microstructure variation as described above.

The $R(H)/R(H{=}O)$ ratios of LSMO and LS–L4 samples, measured at 100 and 300 K, versus the applied field up to 1 T are represented in Fig. 6. A highly resistive grain boundary provides both the tunneling barrier and magnetic decoupling of grains. Below the magnetic field of 1 kOe, the MR value abruptly increases with increasing field, which is related to the LFMR effect. At larger fields (H > 2 kOe), the MR value almost linearly increases with increasing field. The fast resistivity drop in low field is attributed to the magnetic domain alignment. Much slower and linear resistivity drop in high field is due to a forced spin alignment in spin-disordered region near LSMO grain boundary [28]. Thus, two major factors affecting the MR value include the grain boundary areal density and the degree of a disordered region near the grain boundary. In comparison with pure LSMO, the composite samples surely have higher grain boundary areal density because of reduction in average grain size (see Fig. 2) and narrower disordered region near LSMO grain boundary due to the existence of La_2O_3 chemically compatible with LSMO. Therefore, high grain boundary areal density and sharpening of a disordered region near LSMO grain boundary are believed responsible for the enhanced LFMR values of the composite samples. This result is also consistent with that of LSMO–manganite oxide composites of our previous report [26].

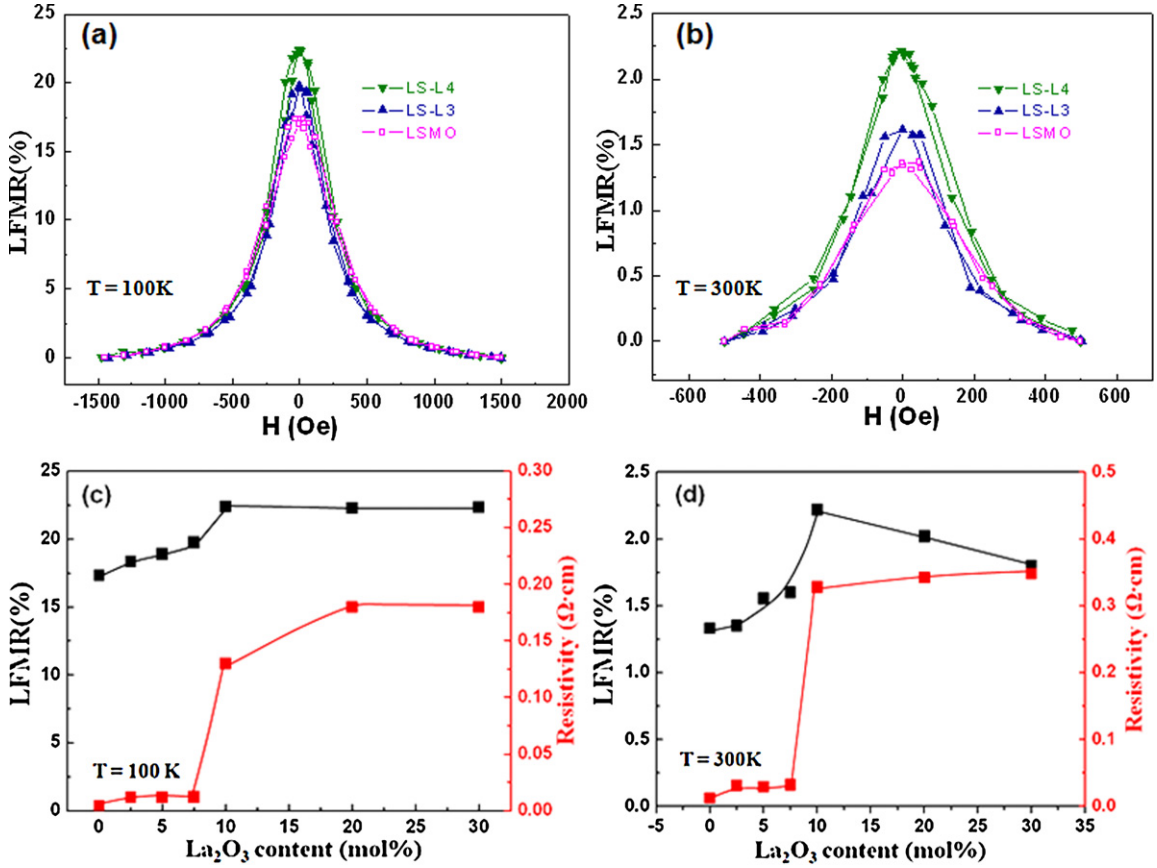

Fig. 5. The LFMR behaviors of some selected samples measured at (a) 100 K and (b) 300 K. The electrical resistivity and maximum LFMR values of all samples are plotted as a function of the La_2O_3 content at (c) 100 K in 1500 Oe and (d) 300 K in 500 Oe, respectively.

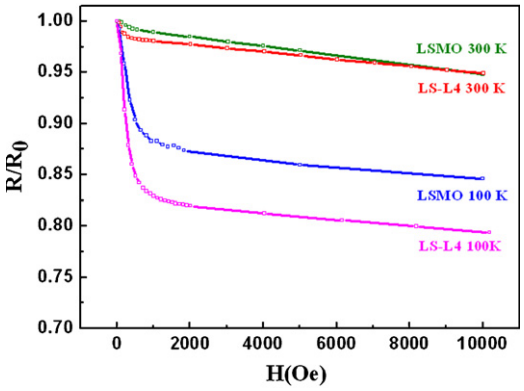

Fig. 6. The $R(H)/R(H=O)$ ratios of LSMO and LS–L4 samples, measured at 100 and 300 K, versus the applied field up to 1 T.

4. Conclusion

The LSMO–La_2O_3 composites were turned out to have excellent LFMR effects at room temperature. The maximum LFMR value of 2.22% at 300 K in 500 Oe could be achieved from the composite sample of 10 mol% La_2O_3 addition. Remarkably improved LFMR properties of the LSMO–La_2O_3 composites in comparison with pure LSMO are attributable to sharpening of disordered LSMO grain boundary region acting as more effective spin-dependent scattering centers. Consequently, the LSMO–La_2O_3 composite is very promising alternative for the MR device application. However, since the La_2O_3 phase is very hygroscopic, the LSMO–La_2O_3 composite can be seriously damaged when it is exposed to humidity in air, and hence surface must be required for a real application.

Acknowledgements

The authors would like to express our thanks to Dr. Young-Min Kang in Samsung electronics for a useful discussion. This work was supported by the Korea Science and Engineering Foundation (KOSEF) grant funded by the Korea government (MEST) (No. KRF-0417-20100021).

References

[1] R. von Helmolt, J. Wecker, B. Holzapfel, L. Schultz, K. Samwer, Phys. Rev. Lett. 71 (1993) 2331.
[2] S. Jin, T.H. Tiefel, M. McCormack, R.A. Fastnacht, R. Ramesh, L.H. Chen, Science 264 (1994) 413.
[3] H.Y. Hwang, S.W. Cheong, N.P. Ong, B. Batlogg, Phys. Rev. Lett. 77 (1996) 2041.
[4] L.L. Balcells, J. Fontcuberta, B. Martínez, X. Obradors, J. Phys.: Condens. Matter 10 (1998) 1883.
[5] M.B. Salamon, M. Jaime, Rev. Mod. Phys. 73 (2001) 583.
[6] A.P. Ramirez, J. Phys.: Condens. Matter 9 (1997) 8171.
[7] J. Coey, M. Viret, S. von Molnar, Adv. Phys. 48 (1999) 167.
[8] Bao-xin Huanga, Yi-hua Liua, Xiaobo Yuana, Cheng-jian Wanga, Ru-zhen Zhanga, Liang-mo Mei, J. Magn. Magn. Mater. 280 (2004) 176.
[9] Anurag Gaur, G.D. Varma, J. Alloys Compd. 453 (2008) 423.
[10] D.K. Petrov, L. Krusin-Elbaum, J.Z. Sun, C. Feild, P.R. Duncombe, Appl. Phys. Lett. 75 (1999) 995.
[11] O.A. Shlyakhtin, K.H. Shin, Young-Jei Oh, J. Appl. Phys. 91 (2002) 7403.
[12] A. Gaur, G.D. Varma, Cryst. Res. Technol. 42 (2007) 164.
[13] L.L. Balcells, A.E. Carrillo, B. Martínez, J. Fontcuberta, Appl. Phys. Lett. 74 (1999) 4014.
[14] Anurag Gaur, G.D. Varma, Solid. State Commun. 139 (2006) 310.
[15] V. Moshinyaga, B. Damaschke, O. Shapoval, A. Belenchuk, J. Faupel, O.I. Lebedv, J. Verbeeck, G. van Tendeloo, M. Mucksch, V. Tsurkan, R. Tidecks, K. Samwer, Nat. Mater. (2003) 247.
[16] Chun-Hua yan, Zhi-Gang Xu, Tao Zhu, Zhe-Ming Wang, Fu-Xiang Cheng, Tun-Hui Huang, Chun-Sheng Liao, J. Appl. Phys. 87 (2000) 5588.
[17] Shilpi Karmakar, S. Taran, B.K. Chaudhuri, H. Sakata, C.P. Sun, C.L. Huang, H.D. Yang, J. Phys. D: Appl. Phys. 38 (2005) 3757.
[18] Caoshui Xionga, Haixin Hu, Yonghong Xiong, Zhenhua Zhang, Houli Pi, Xi Wu, Lijun Li, FenfenWei, Chongfeng Zheng, J. Alloys Compd. 479 (2009) 357.
[19] P.T. Phonga, N.V. Khiem, N.V. Dai, D.H. Manh, L.V. Hong, N.X. Phuc, J. Alloys Compd. 484 (2009) 12.
[20] Yun-Hui Huang, Xing Chen, Zhe-Ming Wang, Chun-Sheng Liao, Chun-Hua Yan, J. Appl. Phys. 91 (2002) 7733.
[21] Jitendra Kumar, R.K. Singh, H.K. Singh, P.K. Siwach, Ramadhar Singh, O.N. Srivastava, J. Alloys Compd. 455 (2008) 289.
[22] P. Kameli, H. Salamati, M. Hakimi, J. Alloys Compd. 463 (2008) 18.
[23] J.-M. Liu, G.L. Yuan, H. Sang, Z.C. Wu, X.Y. Chen, Z.G. Liu, Y.W. Du, Q. Huang, C.K. Ong, Appl. Phys. Lett. 78 (2001) 1110.
[24] Chun-Hua Yan, Feng Luo, Yun-Hui Huang, Xiao-Hang Li, Zhe-Ming Wang, Chun-Sheng Liao, J. Appl. Phys. 91 (2002) 7406.
[25] J.A.M. van Roosmalen, P. van Vlaanderen, E.H.P. Cordfunke, J. Solid State Chem. 114 (1995) 516.
[26] Young-Min Kang, Hyo-Jin Kim, Sang-Im Yoo, Appl. Phys. Lett. 95 (2009) 052510.
[27] L.E. Hueso, J. Rivas, F. Rivadulla, M.A. López-Quintela, J. Appl. Phys. 89 (2001) 1746.
[28] L.L. Balcells, J. Fontcuberta, B. Martínez, X. Obradors, Phy. Rev. B 58 (1998) R14697.